Journal of Sedimentary Research

Journal of Sedimentary Research, 2009, v. 79, 287–301
Research Article
DOI: 10.2110/jsr.2009.035

THE INFLUENCE OF MASS-TRANSPORT-DEPOSIT SURFACE TOPOGRAPHY ON THE EVOLUTION OF TURBIDITE ARCHITECTURE: THE SIERRA CONTRERAS, TRES PASOS FORMATION (CRETACEOUS), SOUTHERN CHILE

DOMINIC A. ARMITAGE, BRIAN W. ROMANS,* JACOB A. COVAULT,* AND STEPHAN A. GRAHAM
Department of Geological and Environmental Sciences, 450 Serra Mall, Building 320, Stanford, California 94305, U.S.A.
e-mail: armitage@stanford.edu

ABSTRACT: **The Upper Cretaceous Tres Pasos Formation, exposed on the Sierra Contreras, southern Chile, provides an exceptional opportunity to document well-exposed depositional relationships between fine-grained mass-transport deposits (MTDs) and overlying turbiditic sandstone deposits in an ancient deep-water slope system. The lateral continuity of the reservoir-scale sandstone-rich facies at this outcrop is controlled principally by surface topography intrinsic to the MTDs, where overlying, conformable sandstone beds pinch out and lap onto the relative topographic highs of the MTD upper surfaces. Turbidite architecture evolves to more laterally continuous, sheet-like deposits as a result of depositional smoothing of MTD topographic relief and diminished confinement. An MTD surface-topography model containing a hierarchy of three fundamental tiers of MTD upper surface topography is identified at the Sierra Contreras and is defined by the maximum values of the horizontal (x) and the vertical (y) dimensions of the topography relative to local elevation. Each tier of the hierarchy is distinguished from the next by approximately one order of magnitude difference in both of the two dimensions. Tier 1 MTD surface topography is up to several meters in magnitude in the x and y dimensions and creates local pockets of ponded sandstone. Tier 2 MTD surface topography is 10 meters to several tens of meters in the x dimension and several meters to several tens of meters in the y dimension. This scale of topography can laterally compartmentalize discrete packages of sandstone. The largest scale of MTD surface topography, Tier 3, is several hundred meters in both the x and y dimensions and can laterally divide (in at least two dimensions) kilometer-scale sediment-gravity-flow conduits, significantly compartmentalizing sandstone deposits. The cyclic packaging of sandstone and MTDs observed at the outcrop suggest the depositional slope profile was adjusting between graded (constructional) and out-of-grade (degradational) conditions in this overall prograding slope system.**

The MTD surface-topography hierarchy presented here is applicable at a range of scales in analogous MTD-dominated deep-water slope environments, from relatively high-resolution ancient outcrops to lower-resolution seismic-reflection-based studies. Whilst the tiers are successively separated by an order of magnitude in size, there is range within the hierarchy with respect to the topographic dimensions facilitating a more flexible comparison of geographically separated MTDs.

INTRODUCTION

Mass movement is defined as the movement of sediment driven directly by gravity rather than by interstitial fluid motion (Middleton and Hampton 1976), and has been argued to be the principal transport process operating on continental slopes (Nardin et al. 1979). The deposits of submarine mass movement (mass-transport deposits or MTDs) are defined by Nardin et al. (1979) to include debris-flow deposits, which are matrix supported and show little preferred fabric, and slides, which are movements of essentially rigid, internally undeformed masses along discrete shear surfaces. MTDs and their associated failure scarps play a primary role in controlling the general distribution and facies architecture of overlying turbiditic sandstone deposits, but the bed-scale relationships between the fine- and coarse-grained deposits is not well documented. Deposition of turbiditic sandstone can be affected by MTDs in the following ways: (1) failure might create accommodation by sediment evacuation (Hackbarth and Shew 1994; Shultz et. al. 2005), creating conduits favorable for focusing turbidity-current flow and deposition; (2) obstacles might be created by the MTDs, which redirect turbidity currents (e.g., Kastens and Shor 1985; Pickering and Corregidor 2005); (3) local topography favorable for sediment ponding might be created by irregular upper surfaces of MTDs (e.g., Shor and Piper 1989; Pickering and Corregidor 2000; Shultz et al. 2005).

Irregular upper surfaces of seafloor MTDs have been documented in a number of datasets, including high-resolution seismic-reflection data (e.g., Hampton et al. 1996; Piper et al. 1997) and petroleum-industry subsurface seismic-reflection data (Moscardelli et al. 2006; Garziglia et al. 2008). Stratified blocks contained within MTDs, but protruding above the surface, have been documented using seismic-reflection data. These blocks contribute to the irregular nature of the top surfaces (e.g., Shor and Piper 1989; Bøe et al. 2000; de Ruig and Hubbard 2006; Hubbard et al. 2008a). These irregular surfaces can have local vertical relief (height) of up to 100 m (McGilvery et al. 2004). In some cases where blocks have slid on the seafloor, whilst entrained within an MTD, they display surface areas of up to 25 km^2 (Lastras et al. 2002). However, the minimum resolvable resolution of petroleum-industry seismic-reflection data (e.g., approximately 30 m maximum vertical) can make it difficult to determine

* Present Address: Chevron Energy Technology Co., 6001 Bollinger Canyon Road, San Ramon, California 94305 U.S.A.

 1527-1404/09/079-287/$03.00

whether the irregular top surface of an MTD is a depositional feature, a result of postdepositional erosion, or a combination of both.

The nature of the bed-scale relationship between fine- and coarse-grained facies with respect to this depositional topography is generally poorly understood, largely owing to: (1) the scarcity of well-exposed fine-grained outcrop sections; (2) the relatively low resolution of exploration-depth 3D seismic-reflection data; and (3) the paucity of core/well control associated with high-resolution seismic-reflection data. Understanding the geometries of MTD failure scarps, the associated deposits, and the distribution of sandy elements, both spatially and temporally, is crucial to understanding the depositional evolution of a deep-water slope environment and is critical towards developing a predictive tool for petroleum reservoir evaluation in such depositionally complex settings.

The Sierra Contreras in the Ultima Esperanza District of southern Chile offers a rare opportunity to better understand the spatial and temporal distribution and the architectural evolution of sandstone in an ancient MTD-dominated, topographically complex deep-water slope environment due to the extent and quality of outcrop exposure. Multiple scales of MTD surface topography, and the effect on turbidite architecture, are recognized in at least two dimensions (from bed scale to reservoir scale) and placed into a hierarchical classification scheme. This scheme ties the bed-scale geometries to explicit lithologic control over several kilometers of outcrop, surpassing the resolution acquired with industry-standard seismic-reflection data and allow for the development of models to explain facies distribution in similar depositional environments.

GEOLOGIC AND STRATIGRAPHIC SETTING

The Cretaceous Magallanes foreland basin is located in the Ultima Esperanza District of southern Chile near the Parque Nacional Torres del Paine (Fig. 1A). Developed as a successor basin built upon the Jurassic Rocas Verdes rift basin, deep-water sedimentation in the Magallanes basin began in the Early Cretaceous related to loading by obducted oceanic crust, which caused flexural subsidence in the retroarc position (Dalziel 1986; Dalziel and Brown 1989; Wilson 1991; Fildani and Hessler 2005). Deep-water sedimentation persisted throughout the Cretaceous, as recorded by the Punta Barrosa and Cerro Toro formations and capped by the slope deposits of the Tres Pasos Formation (Fig. 2; Katz 1963; Scott 1966; Natland et al. 1974; Biddle et al. 1986; Wilson 1991). The overlying uppermost Cretaceous shallow marine and deltaic deposits of the Dorotea Formation record the final filling of the basin (Macellari et al. 1989). Paleocurrent data from these formations indicate a north-to-south transport direction, parallel to the trend of the fold–thrust belt and consistent with a longitudinal basin axis (Fildani and Hessler 2005; Shultz et al. 2005; Hubbard et al. 2008b). Eastward migration of the fold–thrust belt continued into the Tertiary, uplifting the deep-water strata into their present position (Wilson 1991).

The Tres Pasos Formation (1000–1500 m thick) is exposed for more than 100 km in a roughly north–south-trending monocline. The lithostratigraphic base of the Tres Pasos is defined as the first significant sandstone section overlying the shaly upper Cerro Toro Formation (Katz 1963). This study focuses on approximately 500 m of slope deposits of the uppermost Cerro Toro Formation and the lower Tres Pasos Formation, which are superbly exposed at the Sierra Contreras. This outcrop is located in the northern (proximal) Magallanes Basin and records the stratigraphic evolution of an increasingly sand-rich deep-water slope environment (Shultz et al. 2005).

This study builds upon the regional stratigraphic study of Shultz et al. (2005), which recognized two sandstone units on the west face of the outcrop and was limited to only two measured sections. This study incorporates six new measured sections, adding greater detail and lateral control across both the west and the south faces of the Sierra Contreras

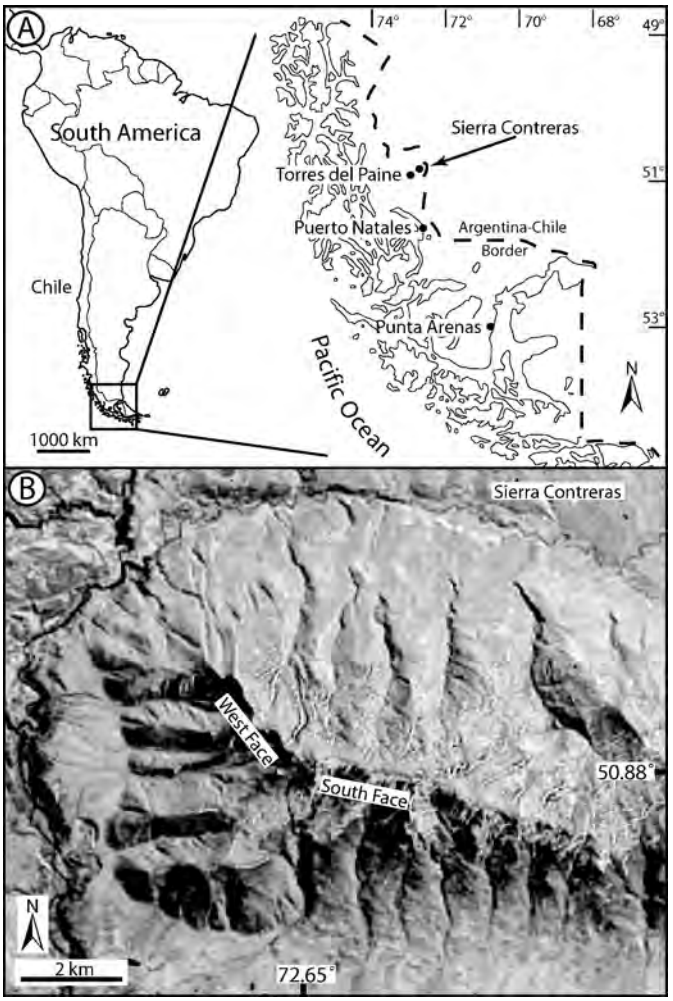

FIG. 1.—**A)** Location map of the study area in southern Chile near the Parque Nacional Torres del Paine. **B)** Satellite image of the Sierra Contreras displaying the location and orientation of the west face and the south face. The west face is approximately 2 km long and trends NW–SE. The south face outcrop is also approximately 2 km long and trends approximately W–E.

(Fig. 1B). This adds an additional dimension to both the stratigraphic interpretation and the model developed at this outcrop.

The west face trends NW–SE and is approximately 2 km in length, displaying a view slightly oblique to depositional dip (paleoflow is approximately to the south; cf. Shultz et al. 2005). The south face trends E–W and is also approximately 2 km long, displaying the most extensive and well-exposed depositional strike view in the Tres Pasos Formation, not previously described. Four sandstone units (10–80 m thick) are defined on the west face (Fig. 3A), Units A–D (oldest to youngest, see Fig. 3B for location of D). Units B and C are the lower and upper sandstone units, respectively, of Shultz et al. (2005). The sandstone units are separated by fine-grained units (96–160 m thick), numbered 1–4 (oldest to youngest), which are dominated by MTDs. Two principal sandstone units are defined on the south face (B′ and C, oldest to youngest, Fig. 3B). Unit B′ is stratigraphically coeval with Unit B; however, MTDs of Units 2 and 3 laterally separate them. Unit C can be traced from the west face to the south face.

METHODS

Approximately 1400 m of detailed measured section (10 cm resolution), photographic documentation, and bed correlations form the

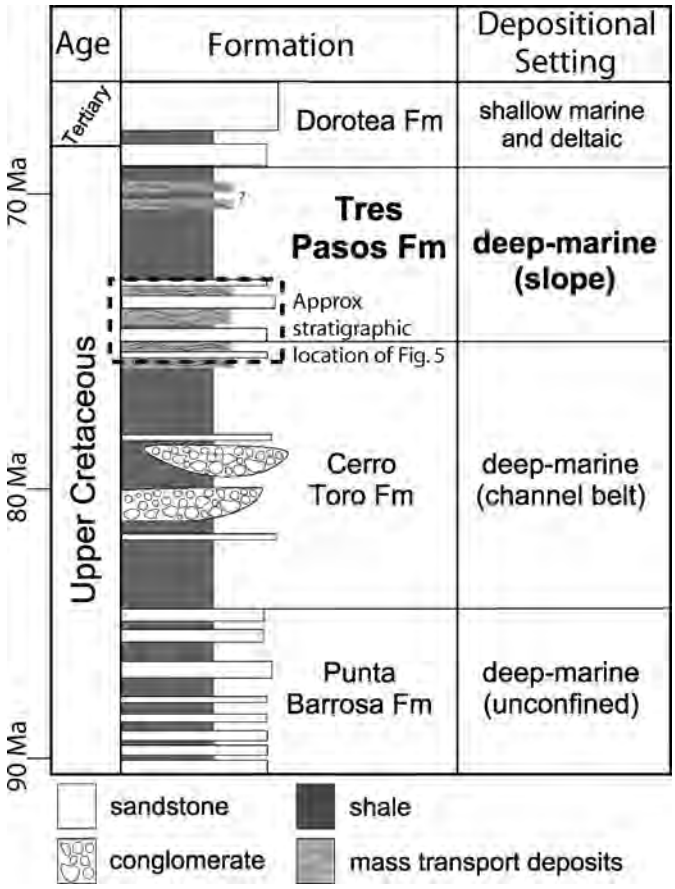

FIG. 2.—Generalized stratigraphic column for the Magallanes foreland basin strata. The Punta Barrosa Formation marks the onset of coarse-grained deep-water sedimentation and initiation of foreland subsidence in the region. Thick, conglomeratic submarine channel-belt deposits characterize the Cerro Toro Formation. The Tres Pasos and overlying Dorotea formations record the culmination of deep-water sedimentation in the basin. An outcrop of slope deposits in the lower part of the Tres Pasos Formation is the focus of this study. Figure modified from Fildani and Hessler (2005). Dashed-line box marks approximate stratigraphic location of Figure 5.

foundation of the dataset. Sections are tied by physically walking out beds and/or photomosaic correlation.

Lithofacies at the Sierra Contreras, described below after Shultz et al. (2005), are defined as groups of genetically related sedimentation units (e.g., beds deposited during an individual sediment-gravity-flow event), which in turn are defined by sedimentary structures (the finest scale of observation). The lithofacies defined here are comparable in scale to the third-order architectural elements of Ghosh and Lowe (1993) and Lowe and Ghosh (2004).

The top surfaces of MTDs are delineated using a hierarchical classification scheme determined by the x and y (i.e., horizontal and vertical, respectively) dimensions of top surface topographic features and the apparent influence on overlying turbidite architectures. Topography is defined as the relative elevations of features on the MTD surface. Each tier in the hierarchy presented here is distinguished from the next by an order of magnitude in the x and y dimensions.

LITHOFACIES

The stratigraphic section exposed at the Sierra Contreras can be subdivided into three lithofacies: (1) medium- to thick-bedded sandstone

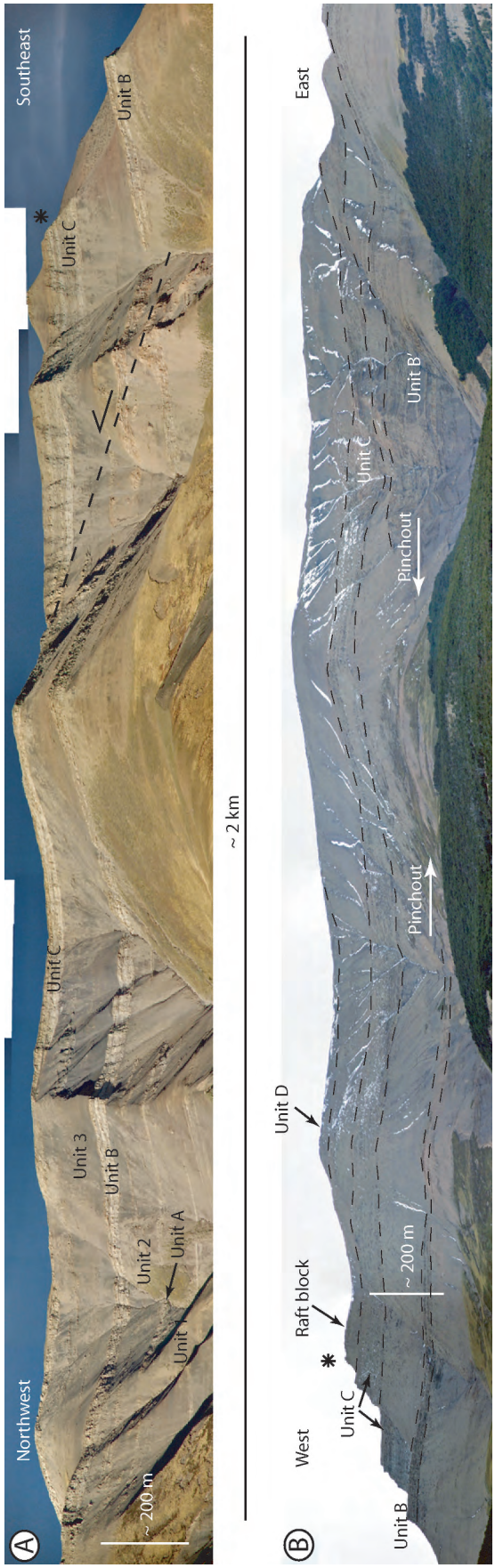

FIG. 3.—**A)** The west face of the Sierra Contreras, with stratigraphic units discussed in this paper delineated. Four fine-grained units are defined on the west face, dominated by MTDs, numbered 1–4. Four coarse-grained units are identified on this face, Units A–D. Approximately 500 m of section is exposed. Paleoflow is approximately to the SSW. **B)** The south face of the Sierra Contreras, with the units delineated. Two coarse-grained units are identified on this face, Units B′ and Unit C. Unit C can be traced across from the west face. Unit B′ is stratigraphically coeval with Unit B, yet laterally separated by MTDs. Star indicates the same geographic point in both photos.

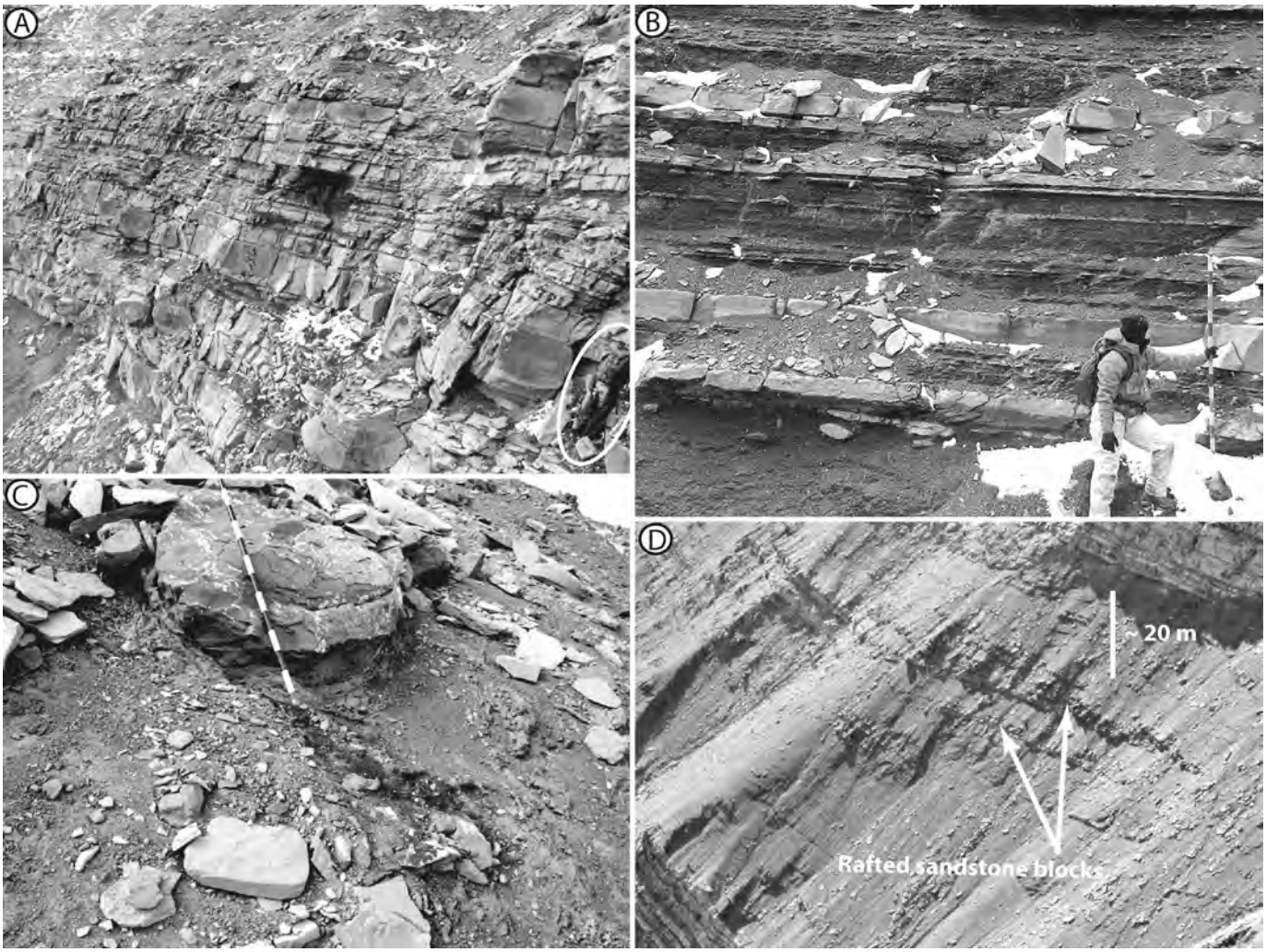

FIG. 4.—**A)** Lithofacies 1 (L-1). Medium- to thick-bedded, non-amalgamated sandstone (person circled for scale). **B)** Lithofacies 2 (L-2). Thin-bedded very fine- to medium-grained sandstone interbedded with shale. **C)** Lithofacies 3 (L-3). A silty debris flow containing a sandstone clast (Jacob Staff is 1.2 m long in this view). **D)** Rafted sandstone blocks in L-3.

(individual beds from 10 cm to 3 m); (2) silty shale and thin-bedded sandstone (individual beds from mm to 10 cm); and (3) chaotic deposits.

Lithofacies 1 (L-1): Medium- to Thick-Bedded Sandstone

Description.—Lithofacies 1 is dominated by medium- and thick-bedded sandstone with thin shale partings (Fig. 4A) and is commonly found to concordantly overlie deposits of Lithofacies 3. Sedimentation units (beds that represent an individual gravity-flow event) are typically 10 cm to several meters thick, are normally graded, and consist of medium-grained sandstone. Individual sedimentation units are commonly characterized by massive bases, which grade normally into planar laminae and are capped by millimeter- to centimeter-scale silty shale. Evidence of minor scour (e.g., flute casts) is common on the soles of sandstone beds. These sedimentation units are generally tabular and can be traced laterally for at least several hundred meters; however, minor scour-filled lenticularity (several meters change in thickness over several hundred meters) is observed near the bases of the sandstone units.

Interpretation.—The thick, medium-grained sedimentation units (> 30 cm) in L-1 are interpreted as the deposits of high-density turbidity currents deposited under waning flow conditions; thinner beds represent the deposits of either low-density or high-density turbidity currents (Bouma 1962; Lowe 1982). The normally graded and planar-laminated divisions of sedimentation units are interpreted as the T_a–T_b Bouma divisions, respectively. The silty shale beds observed in this lithofacies were deposited from suspension and dilute muddy turbidity currents (''background'' deposition). The increased lenticularity of beds at the bases of the sandstone units might suggest increased confinement during deposition. The tabular geometries are indicative of deposition in a relatively unconfined setting.

Lithofacies 2 (L-2): Silty Shale and Thin-Bedded Sandstone

Description.—This lithofacies consists of thinly laminated silty shale interbedded with thin-bedded sandstone beds (Fig. 4B). Sedimentation units are typically several millimeters to 10 cm in thickness and composed of very fine- to medium-grained sandstone. Beds of medium-grained sandstone are generally massive and normally graded. Beds composed of very fine- to fine-grained sandstone are interbedded with shale and commonly show traction structures, and are tabular for at least hundreds of meters. Organic detritus (e.g., wood and plant fragments) is abundant in the finer-grained beds.

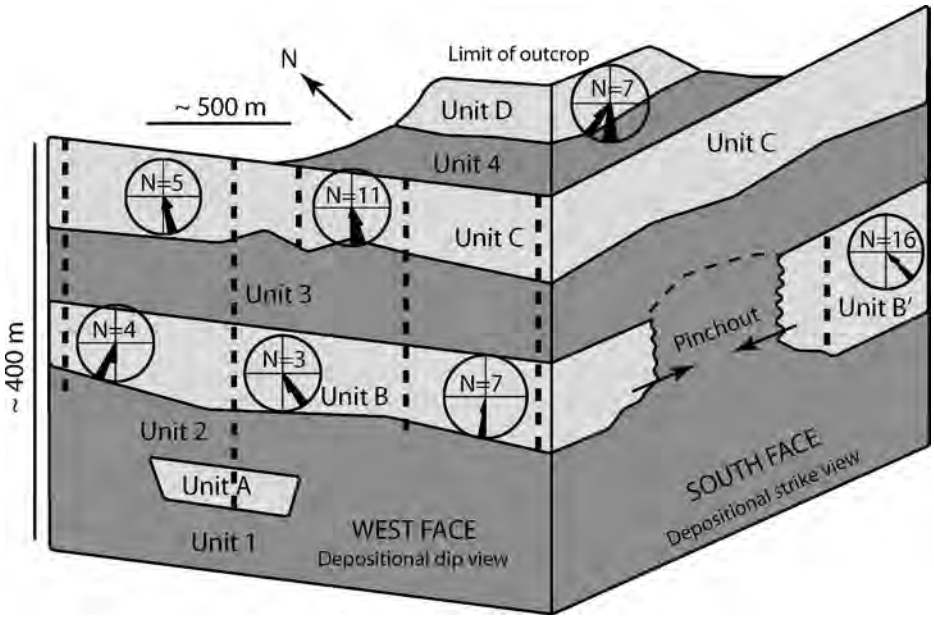

FIG. 5.—Simplified diagram displaying all of the units documented at the Sierra Contreras. Unit C can be traced across both faces. Unit B and B′ are laterally separated by MTDs. Black vertical dashed lines represent the location of the measured sections. The thicknesses of the units are not to scale, and the outcrop is vertically exaggerated. Paleoflow direction of each unit is shown.

Interpretation.—L-2 is interpreted as the deposits of sandy low-density turbidity currents (Bouma 1962), interbedded with silty shale that accumulated from suspension fall out and more dilute turbidity currents.

Lithofacies 3 (L-3): Chaotic Deposits

Lithofacies 3 stratigraphically separates the sandstone units and is responsible for most of the measured stratigraphy at the Sierra Contreras (approximately 70%). The excellent exposure at this outcrop provides an opportunity to further delineate this lithofacies, which aids the analysis of MTD surface topography.

Description.—L-3 is observed between the thick-bedded sandstone of L-1, and is characterized by a poorly sorted silty shale matrix containing deformed sandstone clasts up to several tens of meters in diameter (Fig. 4C). Large (at least 100 m^2 in cross section) sandstone blocks are commonly oriented subparallel to oblique relative to bedding in both the overlying and underlying sandstone units. The blocks are medium-grained sandstone (similar to L-1) and display varying degrees of soft-sediment deformation at their margins. Contacts between L-3 and the underlying sandstone are sharp and relatively planar with only local minor erosion. Conformable contacts between the contorted silty shale of L-3 and overlying sandstone are relatively sharp and irregular, with local topographic relief reaching several meters in the horizontal and vertical dimensions. The margins of this relief do not show evidence of erosion by the overlying sandstone, i.e., there is no truncation of the silty shale beds within the L-3 lithofacies. Where large blocks are observed at the top of L-3 the topographic relief can be up to one order of magnitude larger in the horizontal and vertical dimensions.

Interpretation.—The chaotic deposits of L-3 are interpreted to represent matrix-supported debris-flow deposits. The cohesive freezing of these deposits (Middleton and Hampton 1973, 1976) is thought to be responsible for the minor irregularities of the top surfaces. The structures are frozen examples of those formed during actual flow (Embley 1980). The minor erosion into the underlying sandstone implies conformable debris-flow deposition relatively soon after sandstone deposition (prior to lithification). Where clasts are mappable (at least 100 m^2 in cross section) they are termed "rafts" or rafted blocks (although not strictly occurring at the tops of MTDs, Fig. 4D). The random orientation of these blocks, relative to bedding, suggests that they were supported and rotated by the flow during movement and not solely translated as slide blocks. Rafted blocks are responsible for significant topographic relief (up to several tens of meters in the horizontal and vertical dimensions) on the top surfaces of the chaotic deposits.

STRATIGRAPHIC EVOLUTION OF THE SANDSTONE UNITS

Unit A

Unit A, on the west face of the Sierra Contreras, is the lowest mappable sandstone unit, which marks the onset of relatively significant sandy deposition in this deep-water slope environment (Fig. 5). This unit is 10 m thick and has a relatively sharp contact with the underlying MTDs of Unit 1. Unit A is present only in the northern half of the west face (over approximately 500 m); the coeval stratigraphy on the west face depositionally updip and downdip of Unit A is dominated by MTDs, although the relationship is poorly exposed. There is minimal evidence of erosion into underlying Unit 1. This sand-rich unit is dominated by L-1, with individual beds internally pinching out over approximately 100 m.

Unit B

The fine-grained deposits of Unit 2, underlying Unit B, are approximately 96 m thick where measured, although this thickness is variable (Fig. 6A), and are dominated by L-3. Rafted blocks are more abundant near the top of this unit, creating topographic relief on the MTD top surface. The thickness of overlying Unit B varies from 27 m at the northern end of the Sierra Contreras to 21 m 2 km to the south, reaching a maximum thickness of 34 m in between (Fig. 6A). Unit B displays a thick (approximately 1.5 m) basal succession rich in mudstone clasts that decrease in concentration vertically. The mud clasts are silty and several centimeters in size, with long axes oriented parallel to bedding. Wedging beds are present in the basal sections of this unit, pinching out onto the underlying rugose surface of Unit 2. Unit B is primarily composed of L-1 with approximately 5 m of L-2 dominating the middle of the unit on the west face (Fig. 6A). This section of L-2 can be traced laterally over 1 km on the west face.

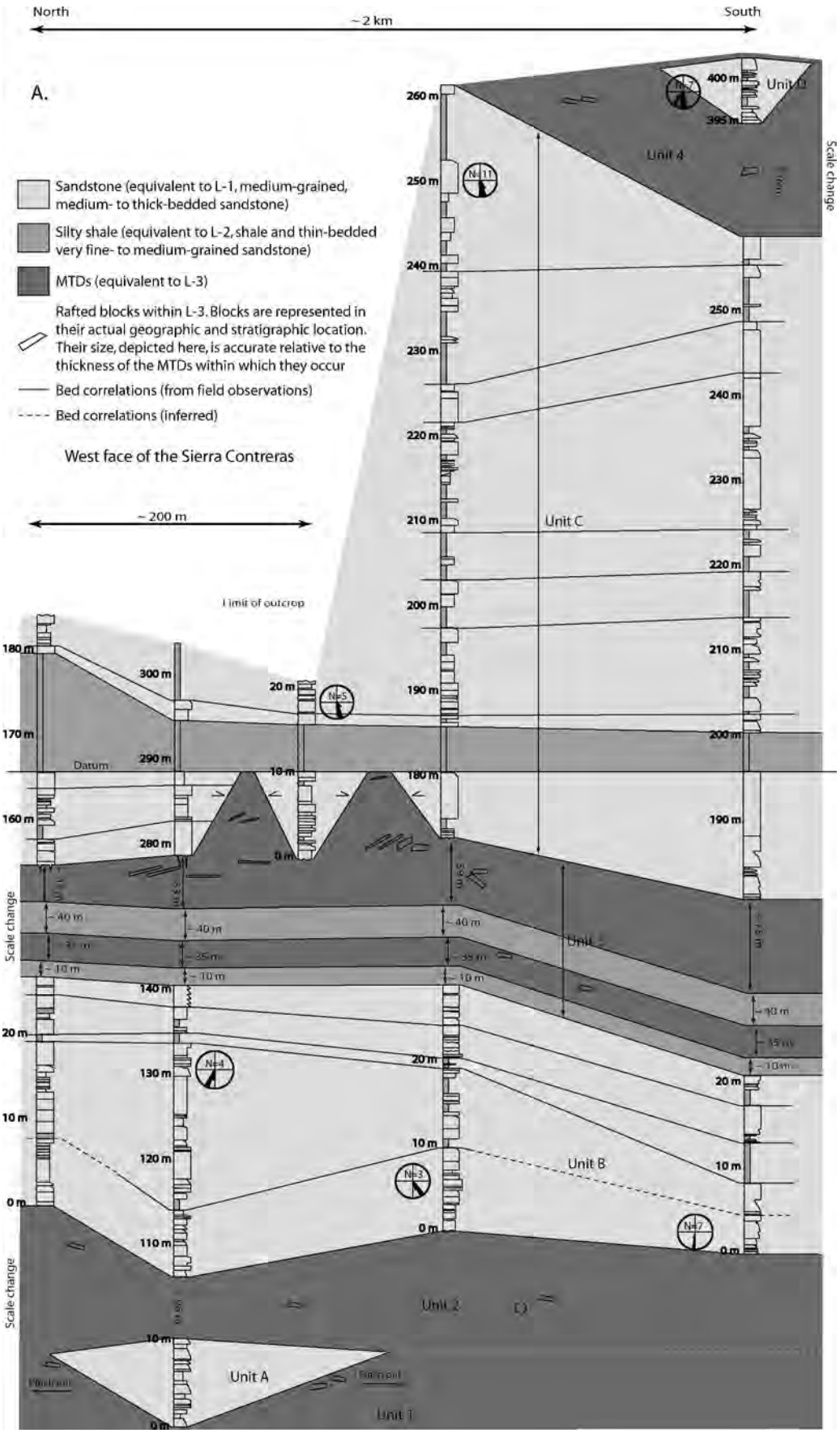
North
~2 km
South
A.
Sandstone (equivalent to L-1, medium-grained, medium- to thick-bedded sandstone)
Silty shale (equivalent to L-2, shale and thin-bedded very fine- to medium-grained sandstone)
MTDs (equivalent to L-3)
Rafted blocks within L-3. Blocks are represented in their actual geographic and stratigraphic location. Their size, depicted here, is accurate relative to the thickness of the MTDs within which they occur
Bed correlations (from field observations)
Bed correlations (inferred)
West face of the Sierra Contreras
~200 m
Limit of outcrop
Datum
Scale change
Unit D
Unit C
Unit B
Unit A
Unit 4
Unit 2
Unit 1
N=7
N=11
N=5
N=4
N=3
N=7

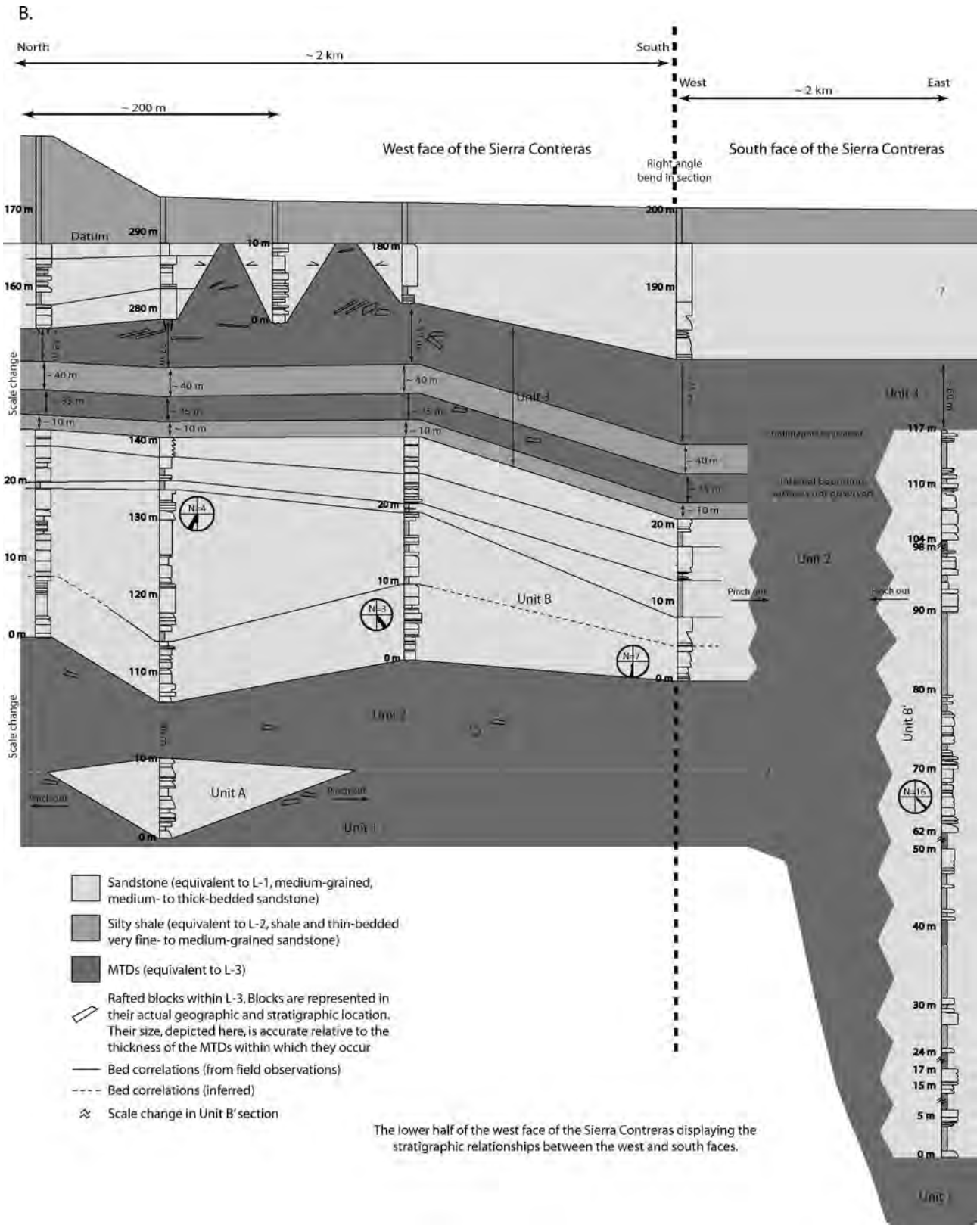

FIG. 6.— **A)** Cross-section (including five measured sections over 2 km) of the west face of the Sierra Contreras (Fig. 3A) with bed correlations and paleoflow measurements. Depositional dip on the cross section is approximately to the south (right). **B)** Cross section correlating the west and south faces at the Sierra Contreras. The west-face cross section has had the top trimmed to accommodate the south face (Fig. 3B) section. See Figure 6A for the entire west-face cross section. Units are correlated between the two faces.

Unit B′

Unit B′ is the lowest and thickest sandstone unit observed on the south face and is approximately 117 m thick (Fig. 6B). The middle of Unit B′ is approximately stratigraphically coeval with Unit B on the west face, yet the two units pinch out toward each other into MTDs (Figs. 5, 6B). L-1 is the dominant lithofacies in Unit B′, which is commonly separated by packages (approximately 10 m thick) of L-2 and L-3. L-3 composes packages about 10 m thick; therefore, they are incorporated into the overall thickness of Unit B′. The position of the section on the west face that is coeval with the basal and topmost parts of Unit B′ is dominated by MTDs (Units 2 and 3, respectively).

Unit C

The fine-grained unit underlying Unit C is Unit 3, which is 128 m thick in the northern part of the west face and gradually thickens to a maximum of 161 m over a distance of 2 km to the south. L-3 dominates this unit; however, there is approximately 10 m of L-2 at the base of the unit and an approximately 40-m-thick section of L-2 approximately 45 m above the base (Fig. 6A). Imbricated rafted blocks within L-3 crop out near the top of Unit 3 (Fig. 6A). These are several hundred square meters in cross section and are observed approximately 400 m down depositional dip from a slump scar documented by Shultz et al. (2005, their fig. 12). Whilst it is likely that, in general, the failure bowl itself creates the largest order of accommodation (cf. Hackbarth and Shew 1994), these blocks create topography at the top of Unit 3 approximately 10 m in the vertical and 50 m in the horizontal dimensions. Approximately 100 m to the north of these blocks, the basal beds of Unit C lap onto a similar scale of topography. The top approximately 60 m of Unit 3 can be traced onto the south face across the top of Unit B′.

Unit C overlies Unit 3 and can be traced across both faces. The erosional top surface of the mountain is on the west face within Unit C, and this unit thickens from 30 m in the north to 87 m where measured in the south (Fig. 6A). Unit C is composed of L-1 with a 6-m-thick section of L-2 10 meters above the base of the unit. This section can be traced across the west face and forms an effective datum for section correlation (Fig. 6A, B).

Approximately 10 m of medium-bedded sandstone beds (L-1) lap onto the underlying topography of Unit 3 associated with imbricated rafted blocks (Fig. 7). The margin between the MTDs and the sandstone dips southeast 13° relative to bedding. Paleoflow is measured between 160° and 180°. The outcrop face trends northwest–southeast, displaying a view oblique to depositional dip. Wedging is locally present in the basal several meters of Unit C, where it is affected by underlying topography (several meters in the x and y dimensions). Turbidite beds, dipping down depositional dip between 3° and 10°, shingle away from the small-scale topography created by the imbricated rafted blocks. The shingled section is approximately 8 m thick with evidence of scour at the top surface. Scour locally incises up to several meters, filled with lenticular beds several tens of centimeters thick in places. The 6-m-thick section of L-2 that can be traced across the outcrop occurs above the shingled bed (Fig. 7). The approximately 15-m-thick section of L-1 sandstone above the fine-grained deposits is tabular and laterally extensive.

Unit D

Unit D overlies the approximately 136-m-thick section of Unit 4. Unit 4 is dominated by L-3 with dispersed rafted blocks throughout. One particular block is coarse grained, several 100 m^2 in cross section and contains a 15-cm-thick bed rich in disarticulated and fragmented shelly material.

The overlying Unit D is approximately 10 m thick and composed of L-1 (Fig. 6A). The unit can be traced for approximately 300 meters before pinching out. This unit is bounded laterally by the underlying MTDs of Unit 4. Minor loading is present at the base of Unit D in addition to downward sandstone injection into the underlying fine-grained deposits. No shale drape or coarse lag deposits are observed between the underlying MTD and the basal sandstone. This unit forms the top surface of the mountain at the corner between the west and south faces (Fig. 5).

DISCUSSION

Surface Hierarchy of Mass-Transport Deposits

The MTDs (i.e., L-3) at the Sierra Contreras display very irregular top surfaces, which are highlighted by the overlying, onlapping sandstone units. MTD surface topography arises from local shaly mounds and rafted sandstone blocks of various sizes (Figs. 8A–D, 9). The paucity of truncated shale on the top surfaces indicates that erosion by subsequent turbidity currents was minimal, although is not entirely discounted.

The first tier of the hierarchy of surfaces relates to topographic features several meters in horizontal and vertical dimensions. Such features are interpreted to be inherent to the viscous nature of cohesive debris flows and form randomly as a result of cohesive freezing (Embley 1980). Overlying sand deposits commonly modified these features by inducing loading. The basal beds (up to several meters) of the overlying sandstone unit pinch sharply toward these features until the topographic depression is filled by sand (Fig. 8A). Sandstone units confined by this small-scale topography are typically wedge-shaped L-1 and laterally discontinuous. Sandstone beds above these deposits are more laterally continuous and confined by the next tier of topographic feature.

The next scale of topographic feature (Tier 2) is one order of magnitude larger (i.e., tens of meters) in the two dimensions observed. This scale of topography on MTD top surfaces is a result of rafted sandstone blocks near or at the top of the chaotic deposits of L-3 (Fig. 8B, C, D). The size of the topography is determined by the size of the rafted block and the degree to which it protrudes above the top surface at the time of deposition. Basal beds of overlying sandstone units pinch toward and lap onto the topographic high formed by the block(s). Similarly to the Tier 1 scale of topography, when the onlapping beds reach the highest point created by the topography the beds become more laterally continuous (sheet-like) as they evolve into relative unconfinement. Such beds are laterally continuous until confined by the next tier of MTD surface topography. The magnitude and abundance of rafted blocks determine the continuity in the basal sections of the sandstone units. Variations in the strength of the debris-flow matrix at the time of deposition might also be an important factor influencing the distribution of large rafted blocks (Kastens and Shor 1985). Although the third dimension of the blocks is not evident at the outcrop, it is assumed to be similar, certainly within an order of magnitude, to the horizontal scale measured (the x axis). This is consistent with rafted blocks resolved in three dimensions (e.g., Shor and Piper 1989; Posamentier and Walker 2006).

The largest scale of MTD surface topography (Tier 3) is one order of magnitude larger than Tier 2 (i.e., hundreds of meters or more) in at least the two dimensions observed, and is interpreted to be the result of an individual MTD (or outsized rafted block) or large-scale hummocky topography on the MTD top surface. From seafloor examples this irregular topography has been documented to reach up to 100 m (McGilvery et al. 2004). Such large-scale features might define bounding margins of sites of slope accommodation, as is the case for Unit B′ (at least in two dimensions) on the south face bounded to the west by Unit 2 (Figs. 3B, 5, 6B). The bounding unit to the east of Unit B′ is not well exposed, yet Unit B′ appears to pinch out over several hundred meters into shale. Unit 2, where it confines Unit B′ to the west has some three dimensionality as it forms a ridge coming out of the mountain several hundred meters. This supports the interpretation of a 3D topographic feature on the seafloor.

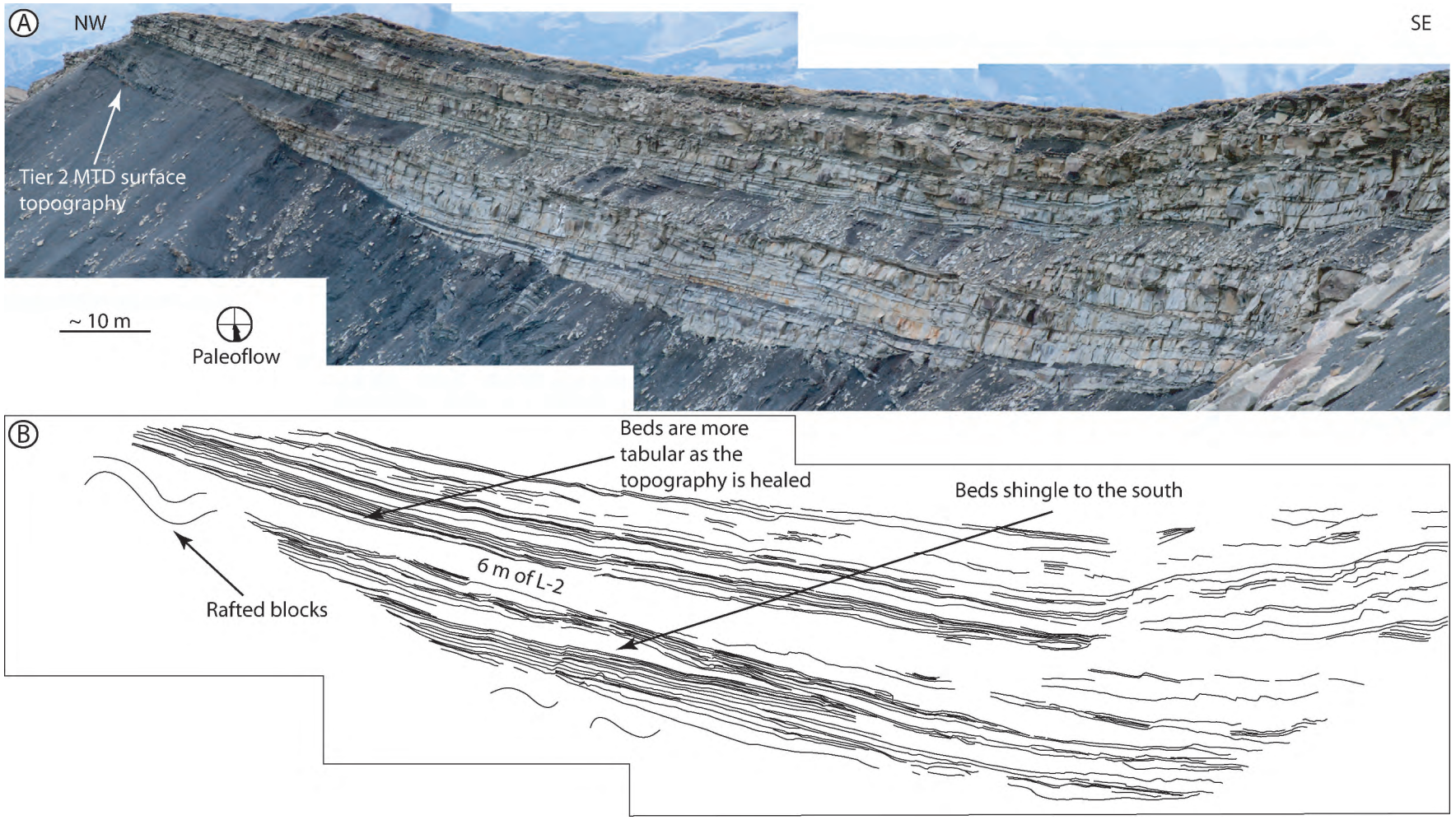

FIG. 7.—**A)** Photomosaic of Unit C affected by the imbricated rafted blocks observed at the top of Unit 3. **B)** A line interpretation of bed architecture in this unit. The lowermost several meters of Unit C fill in Tier 1 MTD surface topography. As the next scale of topography (Tier 2) is filled in, beds shingle to the south. The topography on top of the imbricated blocks is finally smoothed out by a 6 m interval of L-1 that can be traced across the west face. Sandstone beds above this are tabular and laterally extensive.

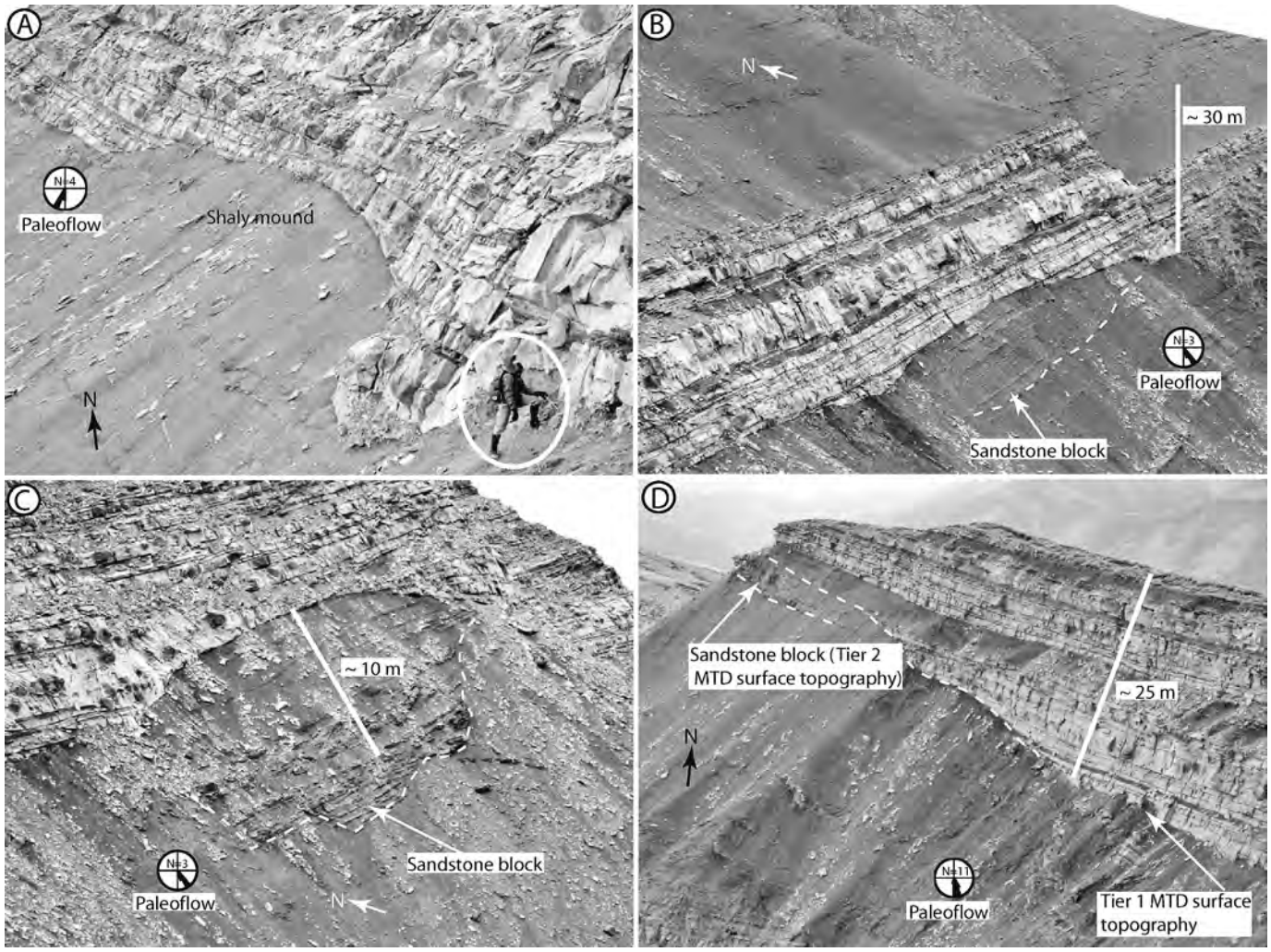

FIG. 8.—Examples of MTD surface topography. **A)** MTD surface topography Tier 1. A shaly mound on the top surface of the MTDs interpreted to have formed by the depositional freezing of a cohesive debris flow. The topography is several meters in both the horizontal and vertical dimensions. Overlying sandstone beds pinch sharply toward and lap onto the feature. **B**, **C**, **D)** Examples of Tier 2 MTD surface topography. Rafted sandstone blocks form this scale of topography. The scale of topography varies from meters to several tens of meters in the vertical dimension and 10 m to several tens of meters in the horizontal dimension. Sandstone beds pinch toward and lap onto the topographic high.

The Influence of MTD Surface Topography on Sand Deposition and Stratigraphic Architecture

Unit A.—The deposits of Unit A represent the fill of a pre-existing sediment dispersal pathway on the MTD top surface, potentially defined by Tier 2 MTD surface topography in the underlying Unit 1, although the margins are poorly exposed. The absence of sandstone loading and the presence of a sharp contact between the fine-grained and coarse-grained deposits suggest some erosion and incision by turbidity currents flowing over the MTD surface; however, truncation of MTD shale is not observed. The wedging observed within this unit is a result of the increased degree of confinement due to the rugose MTD top surface.

Unit B.—The lowest 10 m of Unit B (at the thickest measured point) fills in the accommodation created by several examples of Tier 2 MTD surface topography (Fig. 7B, C, D). This Tier 2 MTD surface topography is healed and beds evolve vertically to more tabular, sheet-like deposits (as documented by Shultz et al. 2005). The variable thickness (21–27 m) of Unit B along the west face (over approximately 2 km) is interpreted to be a result of the undulating surface and the variable thickness of the underlying Unit 2 MTDs. The locally amalgamated package of sandstone in the middle of Unit B on the west face (Fig. 6A, northern part of Unit B) is inferred to represent deposition away from the margins that define the overall accommodation.

Unit B′.—Tier 3 MTD surface topography laterally separates Unit B and Unit B′. The increased thickness of Unit B′ relative to Unit B implies that larger accommodation existed in the area occupied by Unit B′, likely as a result of the variable relief created by the flanks of the local MTD. The presence of this seafloor topography might have deflected and captured an increased number of flows, resulting in the thicker preserved section. The presence of the increased number of thin (approximately 10 m) MTDs within Unit B′ (Fig. 6B) might represent local slumping off of the steep flanks of the bounding MTD or a relatively unstable source area up depositional dip.

Unit C.—The distinct Tier 2 topography at the top of Unit 3 is interpreted to be a result of syn depositional imbricate thrusting along a

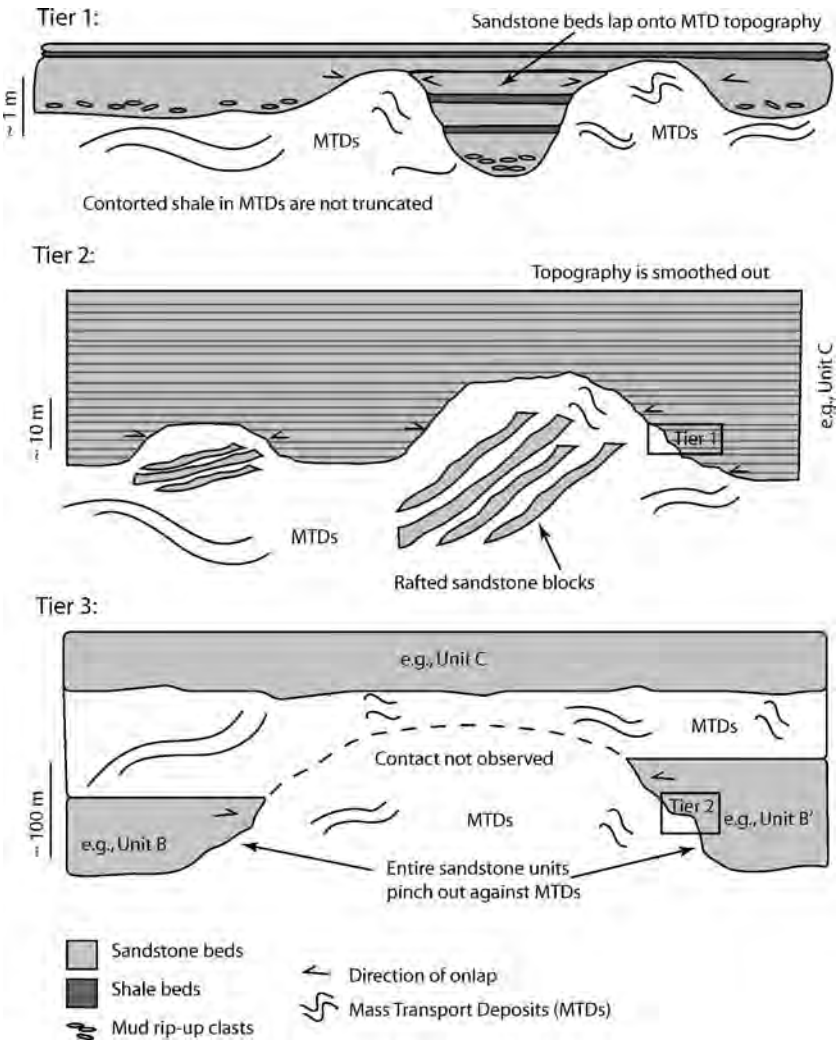

FIG. 9.—Conceptual diagram of the MTD surface-topography hierarchy developed for the Sierra Contreras. Each of the three tiers is shown, outlining the scale and the effect on subsequent turbidite beds. See Table 1 for description. Although the tiers are successively separated by an order of magnitude in size, there is range within the hierarchy with respect to the topographic dimensions, facilitating a more flexible comparison of MTDs.

planar surface and is responsible for locally confining the basal approximately 10 m of overlying Unit C and creating the complex internal architecture (Fig. 7).

This Tier 2 topography created an area of local flow perturbation on the seafloor as turbidity currents were deflected around it. Flow constriction might have occurred if there was similar topography orthogonal to the margin observed. The flow deflection created the oblique-lateral accretion of bar forms shingling away from the margin (Fig. 7). The scour observed at the top of the shingling section is likely to be a product of localized erosion by subsequent sediment gravity flows. The 6 m section of L-2 (Figs. 6A, B, 7) that can be traced across the outcrop indicates that the highest point of the underlying topography had been smoothed out. The lateral continuity of subsequent sandstone beds indicates deposition in an unconfined setting.

Unit D.—The fine-grained unit (Unit 4) underlying Unit D (Fig. 6A) is likely to be an amalgamation of MTDs within the largest order of accommodation; however, potential bounding surfaces, or sections of L-2, are not exposed. The subsequent sandy unit (Unit D) is interpreted as the fill of a narrow conduit on the MTD top surface, potentially bounded by Tier 2 topography (between the west and the south face). The absence of a basal lag deposit or shale drape, and the presence of sandstone loading and injection, indicate conformable deposition.

Slope Evolution and Mass-Transport-Deposit Stacking Patterns

The degree of disaggregation of mass movements generally increases with transport distance if slumps or slides evolve into debris flows down slope (e.g., Mulder and Cochonat 1996; Zhu et al. in press). The cross-sectional size and abundance of rafted sandstone blocks (Fig. 4D) within MTDs at the Sierra Contreras generally increase up section (e.g., Fig. 6A), suggesting that the upper part of the studied interval represents a more proximal position on a generalized slope profile. This progradational signature is consistent with both basin-scale filling patterns of the Tres Pasos and overlying Dorotea formations (Macellari et al. 1989), as well as outcrop-scale stacking patterns documented in the Tres Pasos Formation 20 km to the north (Romans et al. 2008). However, large coherent blocks can be transported long distances (tens of kilometers), both within the flow and as out-runner blocks, and be deposited beyond the base of slope (e.g., Naylor 1982; Hampton et al. 1996; Tripsanas et al. 2008), which, in this case, might suggest a more aggradational stacking pattern. The exceptional lateral exposure at the Sierra Contreras, however, provides additional information supporting the interpretation of basinward stepping in the slope system. The relationship of a failure scar and its associated MTDs approximately 400 m down depositional dip in the upper part of Unit 3 on the west face, first documented by Shultz et al. (2005, their fig. 12), indicates that these blocks were not transported long distances. Furthermore, the presence of the failure scar itself suggests that this was an area of the slope

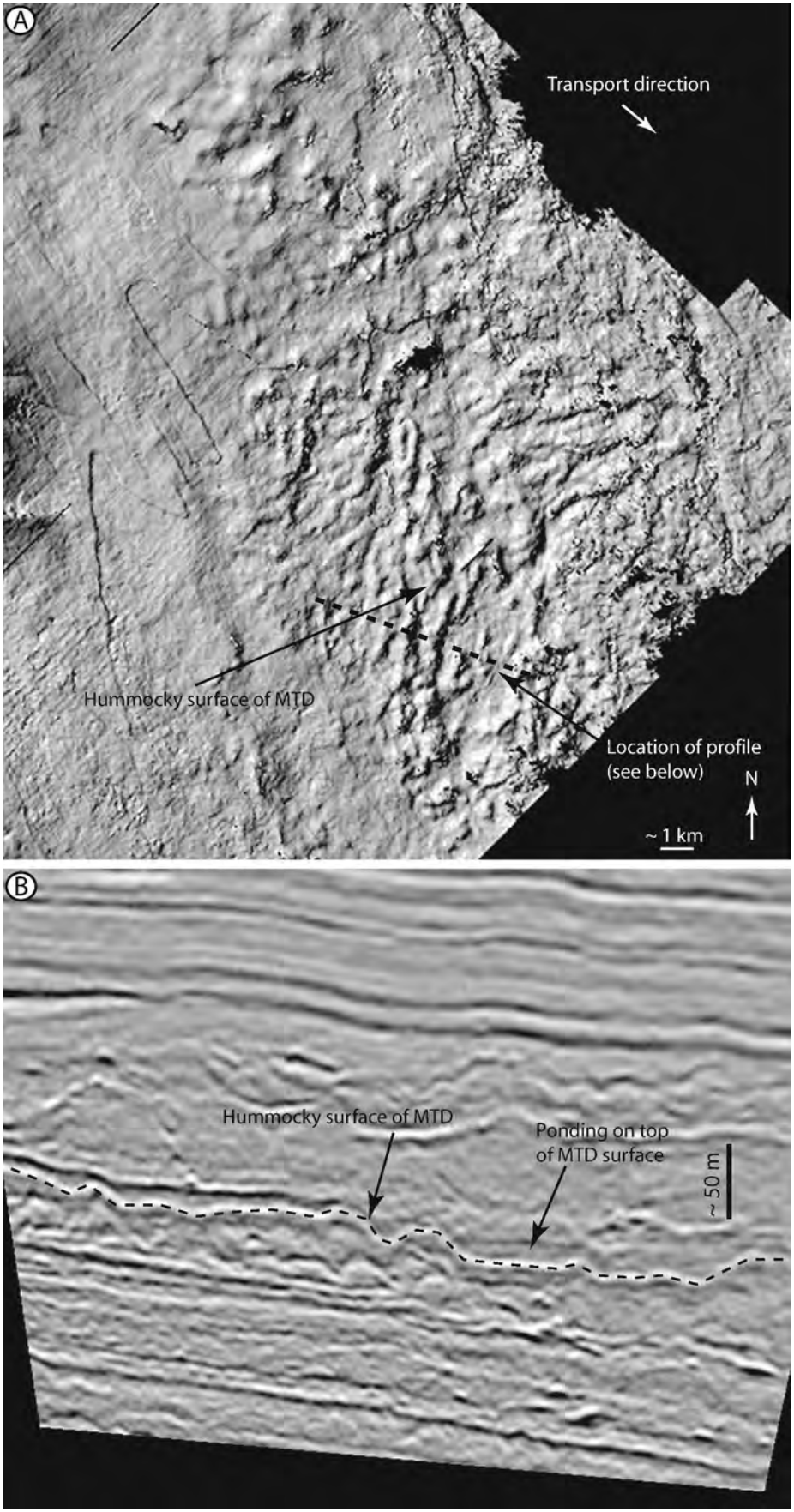

FIG. 10.—**A)** Plan view of the hummocky top surface of a shallow subsurface MTD using petroleum-industry 3D seismic-reflection data. Dashed line marks the location of the profile displayed in Part B. **B)** Seismic-reflection profile taken through the MTD deposits. The surface in Part A is highlighted on the profile. Ponded deposits are observed filling the accommodation created by the irregular surface. Tier 2 MTD surface topography described in this study can describe the MTD surface topography imaged in this view. (Modified from Posamentier and Walker 2006, with permission of SEPM).

TABLE. 1.—*Three tiers of mass-transport-deposit surface topography are defined at the Sierra Contreras. The cause of the topography and the effect on overlying turbidite architecture are outlined. See Figure 9 for the conceptual diagram of the model.*

Horizontal (x) axis of MTD surface topography	Vertical (y) axis of MTD surface topography	Topographic development	Effect on sandstone architecture
Tier 1: Meters to several meters.	Meters to several meters.	Locally irregular nature of the MTD top surface formed as a result of cohesive freezing. May include an element of loading from overlying sandstone.	Creates pods of sandstone on the surface of the MTD, which may enhance foundering. Individual sedimentation units may fill this scale of topography. Sandstone is locally ponded.
Tier 2: 10 m to several tens of meters.	Meters to several tens of meters.	Rafted sandstone blocks.	Basal sections of the sandstone unit lap onto the MTD surface topography. Laterally partitions significant quantities of sandstone (compartmentalizes unit).
Tier 3: 100 m to several hundreds of meters.	100 m to several hundreds of meters.	Individual MTD (or outsized block).	Partitions entire sandstone conduits. Defines units at the outcrop scale. Entire units pinch out against MTD surface topography.

prone to failure. Mass failure and sediment evacuation on an unstable continental slope probably defines the largest order of accommodation at the Sierra Contreras.

Depositional slopes, by definition, record greater accumulation than degradation over time. In the context of continental-margin evolution, Hedberg (1970) and Ross et al. (1994) discussed the distinction between (1) progradational, or graded, margins that advance basinward in equilibrium with external forcings and (2) erosional, or out-of-grade, slopes that become oversteepened, resulting in mass wasting and bypass of sediment to lower-gradient areas. At large stratigraphic scales (hundreds to thousands of meters thick), out-of-grade margins commonly evolve into graded margins as accommodation in lower to base-of-slope areas is filled (Ross et al. 1994). At smaller scales (tens to hundreds of meters thick), the role of degradation vs. accumulation with respect to slope construction is far more complex and thus not as well understood. The scale of stacking of MTD and turbiditic sandstone lithofacies at the Sierra Contreras (Fig. 3A, B) suggests an alternation of graded vs. out-of-grade conditions at a higher temporal order. In this case, the mass-wasting events are critical phases in the evolution and associated accretion of the slope.

Several other prograding slope systems documented from outcrop data exhibit patterns that suggest a dominance of graded conditions (i.e., a paucity of large-scale and numerous intervals of MTDs) (e.g., Eocene strata of Spitsbergen, Steel et al. 2000; Cretaceous Lewis Shale, Pyles and Slatt 2007). Conceptually, a graded slope system builds basinward because the slope profile is maintained at equilibrium (or near equilibrium) during depositional phases. The result is a relatively systematic stacking of facies reflecting their position on the slope (e.g., Plink-Björklund et al. 2001). In contrast, the significant phases recording out-of-grade conditions evident in the Tres Pasos Formation strata suggest a more topographically complex slope profile typical of larger-scale prograding margins (e.g., Moscardelli and Wood 2008).

Comparisons to Stratigraphic Architecture on MTD-Dominated Slopes and Implications for Hydrocarbon Exploration

The creation of a hierarchical classification allows the efficient delineation of the top surfaces of relatively chaotic and internally complex deposits. Such a hierarchy is not restricted to outcrop but can be applied to both modern-day examples on the seafloor and buried examples in the subsurface (Fig. 10). A seafloor example of a blocky debris-flow deposit with high surface roughness has been identified on the Canadian Scotian Slope in about 1500 m water depth on a 2° slope (Shor and Piper 1989). The scale of the topography observed on the top surface of this debris-flow deposit varies between 50 and 200 m in the horizontal and between 5 and 20 m in the vertical, fitting into Tier 2 of the MTD surface-topography hierarchy defined here. The depressions in this debris-flow deposit are filled with subsequent coarse-grained turbiditic sediments, recovered in piston cores (Shor and Piper 1989), similar to the depositional model outlined at the Sierra Contreras, where ponded sand is observed lapping onto topographic highs. The blocks observed in the debris-flow deposit on the Scotian Slope are sourced from the upper slope, with seismic loading as the most likely trigger (cf. 1929 earthquake-induced Grand Banks turbidity current; Doxsee 1948; Piper et al. 1999), factors that might be applicable to the Sierra Contreras with respect to both the source of rafted blocks and possible failure triggering mechanisms. The lower tier (Tier 1) of this hierarchy is most applicable to the interpretation of shallow seismic geomorphology and side-scan sonar and sparker data. Whilst the scale of Tier 3 makes it more suitable for application to petroleum exploration (i.e., industry-standard seismic-reflection datasets) both Tiers 2 and 3 are collectively important for developing (including modeling) reservoirs (Zhu et al. in press).

The relationship between fine-grained chaotic deposits and overlying coarser-grained sandstone deposits are the focus of numerous relatively deep-penetration seismic-reflection-based exploration studies (e.g., in Gulf of Mexico salt-withdrawal minibasins by Prather et al. 1998; Badalini et al. 2000; and Beaubouef and Friedmann 2000; and offshore Trinidad and Tobago by Brami et al. 2000). These studies predominantly focused on external controls (e.g., changes in relative sea level) on the cyclicity of sequences of MTDs overlain by coarser-grained turbidites, and offered brief explanations of controls on turbidite distributions as a result of irregular MTD surface topography. For example, Badalini et al. (2000) presented isochron maps that illustrate topographic compensational filling of a coarse-grained submarine fan overlying an MTD in Basin IV of the Brazos–Trinity system in the Gulf of Mexico. The scales of MTD surface topography correspond with Tiers 2 and 3 of this study. Understanding the scale and distribution of rafted blocks had a large impact on the interpretation of a prospective play. For example, Heritier et al. (1979) initially interpreted the seismically mounded lower Eocene Frigg field (Frigg Formation) to represent the deposits of a submarine fan composed of channels and associated levees. However, Brewster (1991) revised this interpretation to include discontinuous debris-flow deposits. Clearly a more detailed understanding of MTD facies and distribution (within the limits of resolution) could help eliminate such discrepancies and lead to better-informed reservoir models.

Where stratigraphic sequences display similar rugose MTD surface topography overlain by coarser-grained deposits, the hierarchy presented in this study (Fig. 9) can be applied in order to better explain turbidite distribution over a range of scales, and in particular at finer scales than are presented in many previous studies.

CONCLUSION

The Sierra Contreras displays a number of well-exposed MTDs, which are conformably overlain by sandstone units. A combination of cohesive freezing, due to the relatively high viscosity of MTDs, and the size and abundance of the clast (raft) component can lead to a variable top surface on the MTDs during deposition. Where sandy facies are deposited soon after MTD emplacement, this variable MTD surface topography influences the lateral distribution of sandstone beds and might lead to localized compartmentalization of those beds. If the MTD surface topography is substantial enough in both the vertical and horizontal dimensions relative to the surrounding surface, it might serve to confine entire sandstone fairways, leading to a much larger scale of compartmentalization. The sandy facies evolves vertically from a more complicated internal architecture (e.g., wedging or lenticular) nearer the base, as a result of variable confinement, to more sheet-like and laterally extensive beds as the topography is healed and confinement diminishes. The MTD surface topography hierarchy developed from this outcrop, based on the scale and influence of the topography, leads to a better understanding of sandstone distribution and its stratigraphic evolution in depositionally complex environments and will allow for the development of better informed petroleum reservoir models. Furthermore, this dataset adds to our knowledge of the progradation and organization of deep-water slope profiles. The flexibility of the generalized model allows application to a range of datasets at variable scales in depositionally similar yet geographically separated environments.

ACKNOWLEDGMENTS

The authors would like to thank the member companies of the Stanford Project on Deep-water Depositional Systems (SPODDS) for funding this research. These include Aera Energy, Anadarko Petroleum Corporation, Chevron, ConocoPhillips, ENI-AGIP, ExxonMobil, Hess Corporation, Husky Energy, Maersk Oil and Gas, Marathon Oil Company, Nexen Energy, Occidental Petroleum, Petrobras, Reliance Energy, Repsol YPF, Rohol-Aufsuchungs A.G., and Shell. The fieldwork would not have been possible without the fortitude and gallantry of the field assistants, specifically Julie Fosdick and Lisa Stright. Special thanks to Michael Shultz for pioneering the preliminary research during his Ph.D. studies at Stanford University (2000–2004). This paper benefited from numerous discussions with Julian Clark, Andrea Fildani, Zane Jobe, Don Lowe, Tim McHargue, and Henry Posamentier. The authors are grateful for the critical reviews of David Piper, Kevin Pickering, and Associate Editor Kathleen Marsaglia.

REFERENCES

Badalini, G., Kneller, B., and Winker, C.D., 2000, Architecture and processes in the late Pleistocene Brazos–Trinity turbidite system, Gulf of Mexico continental slope, *in* Weimer, P., Slatt, R.M., Coleman, J., Rosen, N.C., Nelson, H., Bouma, A.H., Styzen, M.J., and Lawrence, D.T., eds., Deep-Water Reservoirs of the World: SEPM, Gulf Coast Section, 20th Annual Research Conference, p. 16–34.

Beaubouef, R.T., and Friedman, S.J., 2000, High resolution seismic/sequence stratigraphic framework for the evolution of Pleistocene intra slope basins, western Gulf of Mexico: depositional models and reservoir analogs, *in* Weimer, P., Slatt, R.M., Coleman, J., Rosen, N.C., Nelson, H., Bouma, A.H., Styzen, M.J., and Lawrence, D.T., eds., Deep-Water Reservoirs of the World: SEPM, Gulf Coast Section, 20th Annual Research Conference, p. 40–60.

Biddle, K.T., Uliana, M.A., Mitchum Jr., R.M., Fitzgerald, M.G., and Wright, R.C., 1986, The stratigraphic and structural evolution of the central and eastern Magallanes Basin, southern South America, *in* Allen, P.A., and Homewood, P., eds., Foreland Basins: International Association of Sedimentologists, Special Publication 8, p. 41–63.

Bøe, R., Hovland, M., Instanes, A., Rise, L., and Vasshus, S., 2000, Submarine slide scars and mass movements in Karmsundet and Skudenesfjorden, southwestern Norway: morphology and evolution: Marine Geology, v. 167, p. 147–165.

Bouma, A.H., 1962, Sedimentology of Some Flysch Deposits; A Graphic Approach to Facies Interpretation: Amsterdam, Elsevier, 168 p.

Brami, T.R., Pirmez, C., Archie, C., and Holman, K.L., 2000, Late Pleistocene deep-water stratigraphy and depositional processes, offshore Trinidad and Tobago, *in* Weimer, P., Slatt, R.M., Coleman, J., Rosen, N.C., Nelson, H., Bouma, A.H., Styzen, M.J., and Lawrence, D.T., eds., Deep-Water Reservoirs of the World: SEPM, Gulf Coast Section, 20th Annual Research Conference, p. 104–115.

Brewster, J., 1991, The Frigg field, Block 10/1 UK North Sea and 25/1 Norwegian North Sea, *in* Abbotts, I.L., ed., United Kingdom Oil and Gas Fields, 25 Years Commemorative Volume: Geological Society of London, Memoir 14, p. 117–126.

Dalziel, I.W.D., 1986, Collision and cordilleran orogenesis: an Andean perspective, *in* Coward, M.P., and Ries, A.C., eds., Collision Tectonics: Geological Society of London, Special Publication 19, p. 389–404.

Dalziel, I.W.D., and Brown, R.L., 1989, Tectonic denudation of the Darwin metamorphic core complex in the Andes of Tierra del Fuego, southernmost Chile: implications for Cordilleran orogenesis: Geology, v. 17, p. 699–703.

de Ruig, M.J., and Hubbard, S.M., 2006, Seismic facies and reservoir characteristics of a deep-marine channel belt in the Molasse foreland basin, Puchkirchen Formation, Austria: American Association of Petroleum Geologists, Bulletin, v. 90, p. 735–752.

Doxsee, W.W., 1948, The Grand Banks earthquake of November 18, 1929: Publication of the Dominion Observatory, Ottawa, v. 7, p. 323–335.

Embley, R.W., 1980, The role of mass-transport in the distribution and character of deep-ocean sediments with special reference to the North Atlantic: Marine Geology, v. 38, p. 23–50.

Fildani, A., and Hessler, A.M., 2005, Stratigraphic record across a retroarc basin inversion: Rocas Verdes–Magallanes Basin, Patagonian Andes: Geological Society of America, Bulletin, v. 117, p. 1596–1614.

Garziglia, S., Migeon, S., Ducassou, E., Loncke, L., and Mascle, J., 2008, Mass-transport deposits on the Rosetta province (NW Nile deep-sea turbidite system, Egyptian margin): Characteristics, distribution, and potential causal processes: Marine Geology, v. 250, p. 180–198.

Ghosh, B., and Lowe, D.R., 1993, The architecture of deepwater channel complexes, Cretaceous Venado Sandstone Member, Sacramento Valley, California, *in* Graham, S.A., and Lowe, D.R., eds., Advances in the Sedimentary Geology of the Great Valley Group, Sacramento Valley, California: SEPM, Pacific Section, Guidebook 73, p. 51–65.

Hackbarth, C.J., and Shew, R.D., 1994, Morphology and stratigraphy of a mid Pleistocene turbidite leveed channel from seismic, core, and log data, *in* Bouma, A.H., Weimer, P., and Perkins, B., eds., Submarine Fans and Turbidite Systems: SEPM, Gulf Coast Section, 15th Annual Research Conference, p. 127–133.

Hampton, M.A., Lee, H.J., and Locat, J., 1996, Submarine landslides: Reviews of Geophysics, v. 34, p. 33–59.

Hedberg, H.D., 1970, Continental margins from viewpoint of the petroleum geologist: American Association of Petroleum Geologists, Bulletin, v. 54, p. 3–43.

Heritier, F.E., Lossel, P., and Wathne, E., 1979, Frigg field-large submarine-fan trap in lower Eocene rocks of North Sea: American Association of Petroleum Geologists, Bulletin, v. 63, p. 1999–2020.

Hubbard, S.M., de Ruig, M.J., and Graham, S.A., 2008a, Confined channel–levee complex development in an elongate depo-center: Deep-water Tertiary strata of the Austrian Molasse basin: Marine and Petroleum Geology. doi: 10.1016/j.marpetgeo.2007.11.006.

Hubbard, S.M., Romans, B.W., and Graham, S.A., 2008b, Deep-water foreland basin deposits of the Cerro Toro Formation, Magallanes basin, Chile: architectural elements of a sinuous basin axial channel belt: Sedimentology, v. 55, p. 1333–1359.

Kastens, K.A., and Shor, A.N., 1985, Depositional processes of a meandering channel on Mississippi Fan: American Association of Petroleum Geologists, Bulletin, v. 69, p. 190–202.

Katz, H.R., 1963, Revision of Cretaceous stratigraphy in Patagonian cordillera of Ultima Esperanza, Magallanes Province, Chile: American Association of Petroleum Geologists, Bulletin, v. 47, p. 506–524.

Lastras, G., Canals, M., Hughes-Clarke, J.E., Moreno, A., De Batist, M., Masson, D.G., and Cochonat, P., 2002, Seafloor imagery from the BIG'95 debris flow, western Mediterranean: Geology, v. 30, p. 871–874.

Lowe, D.R., 1982, Sediment gravity flows: II. Depositional models with special reference to the deposits of high-density turbidity currents: Journal of Sedimentary Petrology, v. 52, p. 279–297.

Lowe, D.R., and Ghosh, B., 2004, A stratigraphic and architectural-element methodology for the subdivision and interpretation of deep-water clastic sequences: an example from the Cretaceous Venado Sandstone, Sacramento Valley, California, *in* Appi, C.J., D'Avila, R., and Viana, A., eds., Deep-Water Sedimentation: Technological Challenges for the Next Millennium: Brazilian Association of Petroleum Geologists, Special Paper, p. 42–56.

Macellari, C.E., Barrio, C.A., and Manassero, M.J., 1989, Upper Cretaceous to Paleocene depositional sequences and sandstone petrography of southwestern Patagonia (Argentina and Chile): Journal of South American Earth Sciences, v. 2, p. 223–239.

McGilvery, T.A., Haddad, G., and Cook, D.L., 2004, Seafloor and shallow subsurface examples of mass-transport complexes, offshore Brunei:, Offshore Technology Conference, No. 16780, p. 1–13.

Middleton, G.V., and Hampton, M.A., 1973, Part 1. Sediment gravity flows: mechanics of flow and deposition, *in* Middleton, G.V., and Bouma, A.H., eds., Turbidites and Deep-Water Sedimentation: SEPM, Pacific Section, Short Course Lecture Notes, p. 1–38.

Middleton, G.V., and Hampton, M.A., 1976, Subaqueous sediment transport and deposition by sediment gravity flows, *in* Stanley, D.J., and Swift, D.J.P., eds., Marine Sediment Transport and Environmental Management: New York, Wiley, p. 197–218.

Moscardelli, L., Wood, L., and Mann, P., 2006, Mass-transport complexes and associated processes in the offshore area of Trinidad and Venezuela: American Association of Petroleum Geologists, Bulletin, v. 90, p. 1059–1088.

Moscardelli, L., and Wood, L., 2008, New classification system for mass transport complexes in offshore Trinidad: Basin Research, v. 20, p. 73–98.

Mulder, T., and Cochonat, P., 1996, Classification of offshore mass movements: Journal of Sedimentary Research, v. 66, p. 43–57.

Nardin, T.R., Hein, F.J., Gorsline, D.S., and Edwards, B.D., 1979, A review of mass movement processes, sediment and acoustic characteristics and contrasts in slope and base-of-slope systems versus canyon-fan-basin-floor basins, *in* Doyle, L.J., and Pilkey, O.H., eds., Geology of Continental Slopes: SEPM, Special Publication 27, p. 61–73.

Natland, M.L., Gonzalez, P.E., Canon, A., and Ernst, M., 1974, A System of Stages for Correlation of Magallanes Basin Sediments:, American Association of Petroleum Geologists, Memoir 139, 126 p.

Naylor, M.A., 1982, Debris flow (olistostromes) and slumping on a distal passive continental margin: The Palombini limestone–shale sequence of the northern Apennines: Sedimentology, v. 28, p. 837–852.

Pickering, K.T., and Corregidor, J., 2000, 3D reservoir scale study of Eocene confined submarine fans, south central Spanish Pyrenees, *in* Weimer, P., Slatt, R.M., Coleman, J., Rosen, N.C., Nelson, H., Bouma, A.H., Styzen, M.J., and Lawrence, D.T., eds., Deep-Water Reservoirs of the World: SEPM, Gulf Coast Section, 20th Annual Research Conference, p. 776–781.

Pickering, K.T., and Corregidor, J., 2005, Mass-transport complexes and tectonic control on confined basin-floor fans, Middle Eocene, south Spanish Pyrenees, *in* Hodgson, D.M., and Flint, S.S., eds., Submarine Slope Systems: Processes and Products: Geological Society of London, Special Publication 244, p. 51–74.

Piper, D.J.W., Cochonat, P., and Morrison, M.L., 1999, The sequence of events around the epicentre of the 1929 Grand Banks earthquake: initiation of debris flows and turbidity current inferred from sidescan sonar: Sedimentology, v. 46, p. 79–97.

Piper, D.J.W., Pirmez, C., Manley, P.L., Long, D., Flood, R.D., Normark, W.R., and Showers, W., 1997, Mass-transport deposits of the Amazon Fan: Proceedings of the Ocean Drilling Program, Scientific Results, v. 155, p. 109–146.

Plink-Björklund, P., Mellere, D., and Steel, R.J., 2001, Turbidite variability and architecture of sand-prone, deep-water slopes: Eocene clinoforms in the Central Basin, Spitsbergen: Journal of Sedimentary Research, v. 71, p. 895–912.

Posamentier, H.W., and Walker, R.G., 2006, Deep-water turbidites and submarine fans, *in* Posamentier, H.W., and Walker, R.G., eds., Facies Models Revisited: SEPM, Special Publication 84, p. 399–520.

Prather, B.E., Booth, J.R., Steffens, G.S., and Craig, P.A., 1998, Classification, lithologic calibration, and stratigraphic succession of seismic facies of intraslope basins, deep-water Gulf of Mexico: American Association of Petroleum Geologists, Bulletin, v. 82, p. 701–728.

Pyles, D.R., and Slatt, R.M., 2007, Applications to understanding shelf edge to base-of-slope changes in stratigraphic architecture of prograding basin margins: Stratigraphy of the Lewis Shale, Wyoming, USA, *in* Nilsen, T.H., Shew, R.D., Steffens, G.S., and Studlick, J.R.J., eds., Atlas of Deep-Water Outcrops: American Association of Petroleum Geologists, Studies in Geology 56, CD-ROM, 19 p.

Romans, B.W., Hubbard, S.M., and Graham, S.A., 2008, Stratigraphic evolution of an outcropping continental slope system, Tres Pasos Formation at Cerro Divisadero, Chile: Sedimentology, doi: 10.1111/j/1365-3091.2008.00995.x.

Ross, W.C., Halliwell, B.A., May, J.A., Watts, D.E., and Syvitski, J.P.M., 1994, Slope readjustment: a new model for the development of submarine fans and aprons: Geology, v. 22, p. 511–514.

Scott, K.M., 1966, Sedimentology and dispersal patterns of a Cretaceous flysch sequence, Patagonian Andes, southern Chile: American Association of Petroleum Geologists, Bulletin, v. 50, p. 72–107.

Shor, A.N., and Piper, D.J.W., 1989, A large late Pleistocene blocky debris flow on the Central Scotian Slope: Geo-Marine Letters, v. 9, p. 153–160.

Shultz, M.R., Fildani, A., Cope, T.D., and Graham, S.A., 2005, Deposition and stratigraphic architecture of an outcropping ancient slope system: Tres Pasos Formation, Magallanes Basin, southern Chile, *in* Hodgson, D.M., and Flint, S.S., eds., Submarine Slope Systems: Processes and Products: Geological Society of London, Special Publication 244, p. 27–50.

Steel, R.J., Crabaugh, J., Schellpeper, M., Mellere, D., Plink-Björklund, P., Deibert, J., and Loeseth, T.J., 2000, Deltas vs. rivers at the shelf edge: their relative contributions to the growth of shelf margins and basin-floor fans (Barremian and Eocene, Spitsbergen), *in* Weimer, P., Slatt, R.M., Coleman, J., Rosen, N.C., Nelson, H., Bouma, A.H., Styzen, M.J., and Lawrence, D.T., eds., Deep-Water Reservoirs of the World: SEPM, Gulf Coast Section, 20th Annual Research Conference, p. 981–1009.

Tripsanas, E.K., Piper, D.J.W., Jenner, K.A., and Bryant, W.R., 2008, Submarine mass-transport facies: new perspectives on flow processes from cores on the eastern North American margin: Sedimentology, v. 55, p. 97–136.

Wilson, T.J., 1991, Transition from back-arc to foreland basin development in the southernmost Andes: Stratigraphic record from the Ultima Esperanza District, Chile: Geological Society of America, Bulletin, v. 103, p. 98–115.

Zhu, M., McHargue, T., and Graham, S.A., in press, 3-D seismic-reflection characterization of submarine slides on a Pliocene siliciclastic continental slope and its implications for tectonics, sediment supply, and climate change, South China Sea, *in* Posamentier, H.W., Shipp, C., and Weimer, P., eds., Submarine Slope Systems: SEPM, Special Publication.

Received 28 March 2008; accepted 13 November 2008.